Macromolecules
ARTICLE

Macromolecules **2010**, *43*, 7695–7704 **7695**
DOI: 10.1021/ma101199w

Microphase Separation through Competitive Hydrogen Bonding in Double Crystalline Diblock Copolymer/Homopolymer Blends

Nisa V. Salim,[†] Tracey Hanley,[‡] and Qipeng Guo*,[†]

[†]*Institute for Technology, Research and Innovation, Deakin University, Geelong, Victoria 3217, Australia, and* [‡]*Bragg Institute, Australian Nuclear Science and Technology Organisation, Lucas Heights NSW 2234, Australia*

Received May 29, 2010; Revised Manuscript Received July 30, 2010

ABSTRACT: Microphase separation induced by competitive hydrogen bonding interactions in double crystalline diblock copolymer/homopolymer blends was studied for the first time. Poly(ethylene oxide)-*block*-poly(ε-caprolactone) (PEO-*b*-PCL)/poly(4-vinylphenol) (PVPh) blends were prepared in tetrahydrofuran. The diblock copolymer PEO-*b*-PCL consists of two immiscible crystallizable blocks wherein both PEO and PCL blocks can form hydrogen bonds with PVPh. In these A-*b*-B/C diblock copolymer homopolymer blends, microphase separation takes place due to the disparity in intermolecular interactions; specifically, PVPh and PEO block interact strongly whereas PVPh and PCL block interact weakly. The TEM and SAXS results show that the cubic PEO-*b*-PCL diblock copolymer changes into ordered hexagonal cylindrical morphology upon addition of 20 wt % PVPh followed by disordered bicontinuous phase in the blend with 40 wt % PVPh and then to homogeneous phase at 60 wt % PVPh and above blends. Up to 40 wt % PVPh there is only weak interaction between PVPh and PCL due to the selective hydrogen bonding between PVPh and PEO. However, with higher PVPh concentration, the blends become homogeneous since a sufficient amount of PVPh is available to form hydrogen bonds with both PEO and PCL. A structural model was proposed to explain the self-assembly and microphase morphology of these blends based on the experimental results obtained. The formation of nanostructures and changes in morphologies depend on the relative strength of hydrogen bonding interaction between each block of the block copolymer and the homopolymer.

Introduction

Block copolymers provide a versatile platform for fabricating large-area periodic nanostructures by controlling their self-assembly behavior, with length scales varying from a few nanometers to several hundred nanometers. The repulsive and attractive interactions within and between the blocks as well as their covalent linkage are the driving force for producing self-assembled nanostructures. Block copolymers with the same chemical structure, but different molecular weights and block ratios, provide an effective way to control nanostructure.[1−4] The morphology of block copolymers and development of self-assembled nanostructures have been intensively studied during the past decades, and highly ordered structures such as spheres, cylinders packed in a hexagonal lattice, wormlike micelles, lamellae, and hierarchical nanostructures have been revealed.[5] A binary mixture of self-assembled blends containing a diblock copolymer and a homopolymer can also exhibit well-defined morphologies; these nanostructures are currently being used for many applications such as nanocarriers in drug delivery, gene therapy, diagnostic agents, flocculants, and in pharmaceutical applications.[6−10] The field of block copolymer micelles and their applications have been reviewed extensively by others.[11−24]

Self-assembly of diblock copolymer/homopolymer (A-*b*-B/C) system is a powerful tool for producing functional materials that merge several properties such as reversibility, control of composition, and concurrent self-assembly behavior. Such systems may provide new opportunities for the tailoring of novel tunable functional materials with new properties such as improved processing, self-healing behavior, or stimuli responsiveness. In recent years, attention has mainly focused on the polymer blends with noncovalent physical interactions, such as ionic or electrostatic and hydrogen bonding interactions.[25]Among these, hydrogen bonding interactions in the polymer blends promote the formation of self-assembled structures and different phase transitions that may lead to the production of highly functional polymeric materials. Morphological changes due to hydrogen bonding between amphiphilic block copolymers and a homopolymer were studied by several groups.[26−28] The hydrogen bonding and nanostructure morphologies formed by the hydrogen bonding interaction between a small molecule and block copolymer were extensively investigated by Ikkala's group.[29]

Guo et al.[30] and Chang et al.[31] recently reported the self-assembled block copolymer blends and complexes involving competitive hydrogen bonding interactions between different block copolymer blocks and the homopolymer. This new strategy for the design of nanostructures is based on the competition between different blocks of the block copolymer forming more than one kind of intermolecular interactions with the complementary polymer, leading to a highly stable blend or complex compared to analogous systems which involve elaborate syntheses and multistep preparation protocols. It is proven that careful selection of the polymers, specifically the block copolymer, molecular weight, and the experimental conditions, can lead to self-assembled structures in blends and complexes. Such self-assembled blends involving selective hydrogen bonding could be used for the fabrication of hierarchical and functional materials.

The interaction between different chains in A-*b*-B/C block copolymer/homopolymer mixtures can be characterized by the Flory−Huggins interaction parameter (χ).[32] Various studies have been conducted in such systems, wherein χ between the interacting polymers (χ_{AC}, χ_{BC}, or χ_{AB}) are either positive or negative and

*Corresponding author: tel +61 3 5227 2802; fax +61 3 5227 1103; e-mail qguo@deakin.edu.au.

Published on Web 08/13/2010

can provide more interesting combinations for blending. In A-*b*-B/C type multicomponent systems characterized by a multitude of parameters (χ, chain lengths, and statistical segment lengths), methods for identifying the subset of parameters that govern the thermodynamics of mixing have not been established.[33] Amphiphilic diblock copolymers consist of two chemically dissimilar polymer chains, A and B, covalently bonded at one end, and they have an inherent tendency to self-assemble into tunable nanostructures. Mutual repulsion resulting from the immiscibility of A and B drives the system to segregate. The chains will organize themselves such that A and B blocks are on opposite sides of an interface, with the specific equilibrium nanodomain morphology determined by the degree of polymerization, N, χ, and the relative length of the two blocks, f. The interaction of homopolymer C to the block copolymer depends on the chemical composition and strength of hydrogen bonding between the block copolymer and homopolymer.

Block copolymers self-assemble to form nanostructures via the process of microphase separation which is driven by the enthalpy of demixing of the block copolymer components. This enthalpy is proportional to the product χN.[33] Depending upon the value of χN, it is possible to determine the degree of microphase separation of the diblock copolymer. There are many theories regarding the microphase separation in block copolymer/homopolymer systems. One of them is random phase approximation (RPA), where χ denotes repulsive (bad) interactions ($\chi > 0$) and ξ represents attractive (good) interactions ($\xi < 0$) are the two interaction parameters using for characterizing such systems. Hellmann et al.[33] studied that there is always a repulsive interaction between the homopolymer and one block of the block copolymer ($\chi > 0$) which induces the microphase separation avoiding the homogeneous state or macropahse separation.

For small values of χN, the copolymer and homopolymer are completely miscible, and they always produce a single homogeneous disordered (DIS) phase. Matsen found that the addition of high molecular weight homopolymer leads to macrophase separation between a diblock-rich ordered phase and a homopolymer-rich disordered phase.[34] This macrophase separation was attributed to an attractive interaction between diblock bilayers. However, low molecular weight homopolymer produced a repulsive interaction between bilayers, resulting in an entirely different behavior. There is, however, an increasing interest in block copolymer/homopolymer blends wherein the χ parameters are both positive and negative. In the present A-*b*-B/C systems, the interaction parameter, χ_{AB}, is positive (A and B are immiscible) and ξ_{AC} and ξ_{BC} are negative, but $\xi_{AC} \ll \xi_{BC}$.

The A-*b*-B/C systems involving competitive hydrogen bonding investigated so far consist of block copolymer with two amorphous blocks[30c,31b,c] or amorphous−crystalline blocks.[30a,b,31a] Very recently, Guo and co-workers[35] have investigated microphase separation induced by competitive hydrogen bonding in A-*b*-B/C diblock copolymer/homopolymer complexes where the diblock copolymer A-*b*-B is immiscible and the homopolymer C can interact unequally with both A and B blocks through hydrogen bonding. The hydrogen bonding interactions were analyzed in terms of the difference in interassociation constants (K), i.e., interaction parameters of each blocks of the block copolymer to the homopolymer and according to the random phase approximation. It has been established how hydrogen bonding determines the self-assembly and causes morphological transitions in different A-*b*-B/C diblock copolymer/homopolymer systems with respect to the K values. Nevertheless, blends in which both components of the diblock copolymer are crystalline (double crystalline) have never been studied to the best of our knowledge. In block copolymers containing crystallizable components, the interplay between crystallization and microphase separation strongly influences the structural changes, morphology, properties, and applications of such materials. It is more complicated and interesting to investigate the blends of two crystalline blocks as both components are capable of crystallization and provide various conditions to study the morphology and crystallization behavior in polymer blends.

In the current work, we present for the first time a study of microphase separation induced by competitive hydrogen bonding in self-assembled double crystalline block copolymer/homopolymer blends. In particular, the self-assembly, hydrogen bonding interactions, crystallization, phase behavior, and morphology of poly(ethylene oxide)-*block*-poly(ε-caprolactone) (PEO-*b*-PCL)/poly(4-vinylphenol) (PVPh) blends are investigated. The diblock copolymer A-*b*-B is immiscible, and the homopolymer C can interact with both A and B blocks, but unequally due to the competitive hydrogen bonding interaction between the A/C and B/C pairs. The results are correlated with the phase behavior of the blends experimentally obtained with small-angle X-ray scattering (SAXS) and transmission electron microscopy (TEM). This work for the first time demonstrates how the competitive hydrogen bonding determines the self-assembly and causes morphological transitions in A-*b*-B/C double crystalline diblock copolymer/homopolymer blends.

Experimental Section

Materials and Preparation of Blends. Poly(4-vinylphenol) (PVPh) with an average molecular weight M_w of 20 000 and a polydispersity M_w/M_n of 1.70 was obtained from Aldrich Chemical Co., Inc. The block copolymer used in the present study, poly(ethylene oxide)-*block*-poly(ε-caprolactone) (PEO-*b*-PCL), was purchased from Polymer Source Inc. with M_n-(PEO) = 15 000, M_n(PCL) = 25 000, and M_w/M_n = 1.17. All these polymers were used as received. The blends of PEO-*b*-PCL/PVPh were prepared by solution mixing. Tetrahydrofuran (THF) solution containing 1% (w/v) of the individual polymers were mixed and stirred well until a clear solution was obtained. The solvent was allowed to evaporate slowly at room temperature. The blends were dried under vacuum for 72 h before the measurements in order to reach equilibrium.

Fourier Transform Infrared (FTIR) Spectroscopy. The FTIR spectra of all the samples were measured on a Bruker Vetex 70 FTIR spectrometer. The spectra of all the samples were determined by using the conventional KBr disk method. The THF sample solution was cast onto KBr pellets and dried under vacuum at 80 °C to completely remove the solvent and then allowed to cool to room temperature. The spectra were recorded at the average of 32 scans in the standard wavenumber range of 400−4000 cm^{-1} at a resolution of 4 cm^{-1}.

Differential Scanning Calorimetry (DSC). The glass transition temperatures of the blends were determined by a TA Q200 differential scanning calorimeter using 5−10 mg of the sample under a nitrogen atmosphere. A heating rate of 10 °C/min was employed. All the samples were first heated to 150 °C and kept at that temperature for 3 min, subsequently cooled to −70 at 10 °C/min, held for 5 min, and heating continued from −70 to 200 °C. The midpoints of the second heating scan of the plot were taken as the glass transition temperatures (T_gs).

Polarized Optical Microscopy (POM). Spherulite growth was studied using a Nikon polarizing optical microscope with the Nikon Digital Sight DS-5*M*-U1 system. The polymer sample, sandwiched between two glass slides, was first dried under vacuum at 50 °C for about 48 h, melted at 100 °C for 5 in, then quenched to 25 °C, and annealed at 25 °C for 4 h.

Transmission Electron Microscopy (TEM). TEM experiments were performed on a JEOL JEM-2100 transmission electron microscope at an acceleration voltage of 100 kV. The samples were cut into ultrathin sections of ~70 nm thickness at room temperature with a diamond knife using a Leica EM UC6 ultramicrotome machine. The bulk samples were annealed at 180 °C for about 48 h before microtoming. The thin sections were stained by ruthenium tetraoxide before TEM observation.

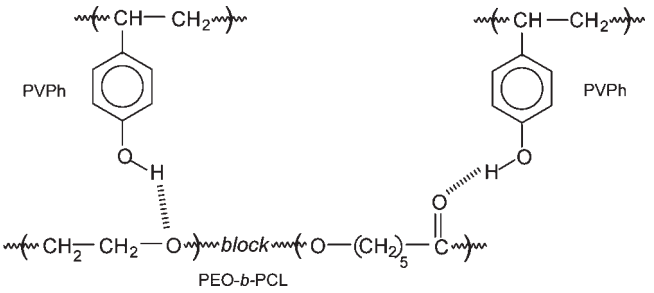

Figure 1. Schematic representation of possible hydrogen bonding interactions between PEO-*b*-PCL diblock copolymers and PVPh homopolymer.

Wide-Angle X-ray Scattering (WAXS). Wide-angle X-ray scattering (WAXS) analyses were carried out using a Panalytical XPert Pro XRD machine. The scanning angle 2θ, from 5° to 35°, was swept at a speed of 0.02/s. The polymer thin films were fixed on the equipment, and the data were collected with every 0.02°.

Small-Angle X-ray Scattering (SAXS). The SAXS measurements were taken on a Bruker NanoStar 3 pinhole small-angle X-ray scattering instrument. Two-dimensional scattering patterns were recorded using a Vantec detector. Annealed samples having 1 mm thickness were prepared for SAXS measurements, and all the experiments were carried out at room temperature (25 °C) as well as at 100 °C using Cu Kα radiation (λ = 1.54 Å, wavelength). The intensity profiles were interpreted as the plot of scattering intensity (I) versus scattering vector, $q = (4/\lambda)\sin(\theta/2)$ (θ = scattering angle).

Results and Discussion

Hydrogen Bonding Interactions. FTIR spectroscopy is an excellent tool for detecting carbonyl, hydroxyl, and ether vibrations.[36] This technique provides (i) information on specific interaction between PEO-*b*-PCL/PVPh blends and (ii) means for studying the mechanism of interpolymer miscibility through the formation of hydrogen bonding both quantitatively and qualitatively. Figure 1 shows the possible specific interaction in the PEO-*b*-PCL/PVPh blends. PVPh has an excellent potential as a proton donor for hydrogen bonding interactions with proton-acceptor polymers because the hydroxyl group of the repeating unit is easily acceptable in the 4-position of the aromatic ring. As shown in Figure 2, pure PVPh exhibits two bands in the hydroxyl stretching region. The self-associated hydroxyl group absorption is located at 3352 cm^{-1}, which is mainly due to the wide distribution of hydrogen bonded hydroxyl groups (self-associated). The free hydroxyl groups give a band at 3525 cm^{-1}, but as the concentration of the block copolymer in PEO-*b*-PCL/PVPh increases, the intensity of this band decreases and finally disappears, implying the formation of hydrogen bonding between the hydroxyl group of PVPh and PEO-ether and PCL-carbonyl groups.

Meanwhile, the self-associated hydroxyl regions of PVPh at 3352 cm^{-1} shift toward lower frequencies with increasing PEO-*b*-PCL content. The peak at 3325 cm^{-1} in 90/10 PEO-*b*-PCL/PVPh blends corresponds to the intermolecular hydrogen bonding interaction between hydroxyl groups of PVPh and ether and/or carbonyl groups of the block copolymer. Table 1 shows the average strength of the intermolecular interaction, which is a measure of the frequency difference (Δv) between the free hydroxyl region and that of the hydrogen bonded species.[37] The Δv values of PVPh/PCL (105 cm^{-1})[38] and PVPh/PEO (295 cm^{-1})[39] binary blends are also given for comparison. This observation implies that the average strength of the hydrogen bond between PVPh hydroxyl group and

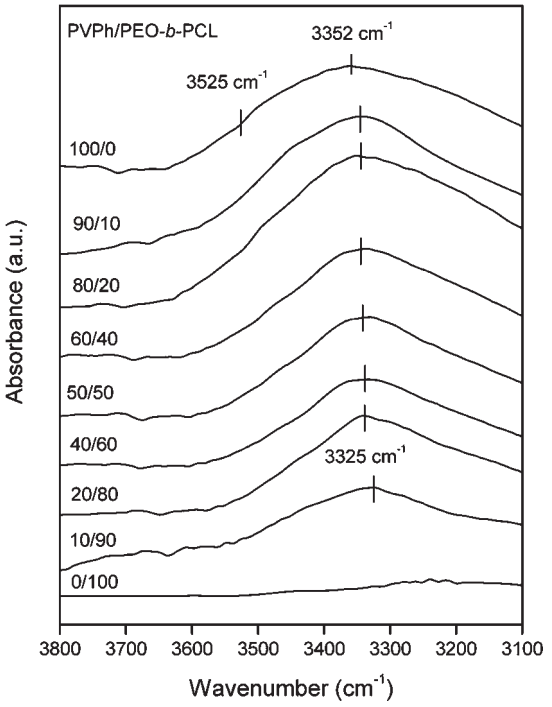

Figure 2. Hydroxyl region of PEO-*b*-PCL/PVPh blends in the infrared spectra observed at room temperature.

Table 1. Wavenumber Shift of Hydroxyl Region in PEO-*b*-PCL Containing PVPh

system	Δv (cm^{-1})
PVPh	173
PVPh/PEO	295[a]
PVPh/PCL	105[b]
PEO-*b*-PCL/PVPh	200

[a] Reference 39. [b] Reference 38.

PEO-*b*-PCL block copolymer (200 cm^{-1}) is higher than that between self-associated hydroxyls in pure PVPh (173 cm^{-1}). However, this value is less than the interassociation between PVPh and PEO (295 cm^{-1}). This method also reveals the hydrogen bonding strength of PEO-*b*-PCL/PVPh blends. The analysis of the Δv values of pure PVPh, PVPh/PEO, and PVPh/PCL reflects that PEO and PCL are both capable of making hydrogen bond with PVPh, although the resulting bond strengths are unequal. The above results imply that the interassociation hydrogen bonds between PVPh and PEO are stronger than the so-called interassociation PVPh/PVPh and PVPh/PCL hydrogen bonds.

Figure 3 represents the FTIR spectra of CH_2 wagging of PEO ranging from 1380 to 1320 cm^{-1}. The PEO spectra show two bands at 1360 and 1343 cm^{-1} corresponding to crystalline phase of PEO.[40] As can be seen in Figure 3, the spectra of the blends show significant changes in this region, suggesting a retardation of PEO crystallization by the addition of PVPh. When the PVPh content in the blend increases, these bands are replaced by a broad band centered at 1350 cm^{-1} which represents the amorphous phase. This result indicates that the hydrogen bonding interaction between PVPh hydroxyl and PEO ether is very strong and exists at all compositions of PVPh.

Figure 4 shows the infrared spectra of the carbonyl stretching region recorded at room temperature ranging from 1660 to 1780 cm^{-1}. The IR spectra of pure PCL exhibits two peaks: a sharp band centered at 1725 cm^{-1} corresponds to PCL in its crystalline conformation, and a shoulder band at

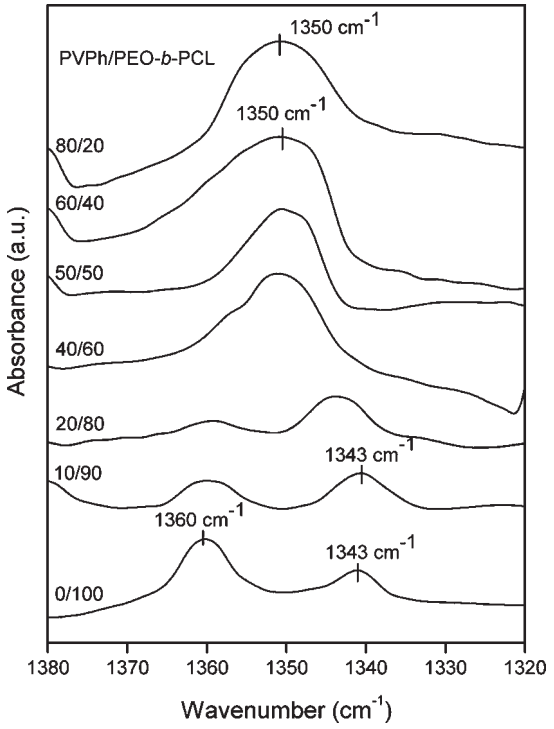

Figure 3. FTIR spectra corresponding to the ether region of PEO-*b*-PCL/PVPh blends at room temperature.

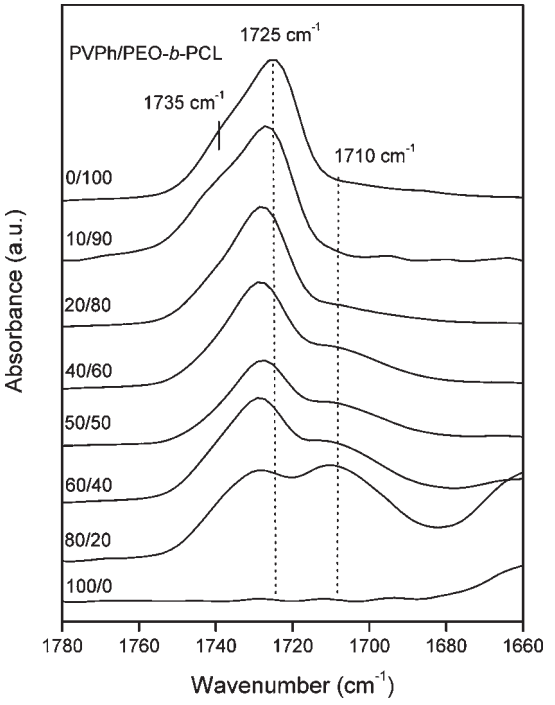

Figure 4. FTIR spectra in the carbonyl region of PEO-*b*-PCL/PVPh blend at room temperature.

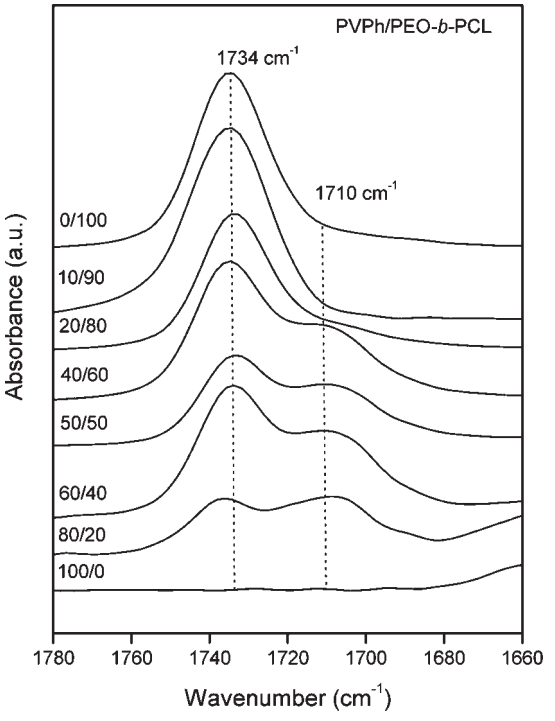

Figure 5. Carbonyl stretching region of PEO-*b*-PCL/PVPh blendes at 75 °C.

1735 cm^{-1} is attributed to amorphous PCL.[41] As the content of PVPh increases in the blends, another band contribution is observed at 1710 cm^{-1}; the presence of this band confirms the vibration of hydrogen bonded carbonyl groups. This band appears in the blends when the PVPh concentration is above 20 wt %. This indicates that the interaction between PVPh and PCL starts when the PVPh concentration is above 20 wt %. Here the intensity increases very slowly with increase in PVPh concentration compared to the free carbonyl band. This signifies that the fractions of hydrogen bonded carbonyl group in PEO-*b*-PCL/PVPh blends are less at lower PVPh concentrations. This is mainly due to the strong hydrogen bonding ability of PEO with PVPh compared to PCL.

The hydrogen bonding interaction of PVPh and PCL was also examined at higher temperature. Figure 5 shows the FTIR spectral changes of PEO-*b*-PCL/PVPh blends in the carbonyl stretching region at 75 °C, above the melting point of PCL. The hydrogen bonded carbonyl band appears approximately at 1710 cm^{-1}. The crystalline peak of PCL centered at 1725 cm^{-1} has vanished here because of the melting of the crystalline components of the block at higher temperature. The prominent feature of these spectra is that the intensity of 1710 cm^{-1} band increases with increasing concentration of PVPh.

Again, quantitative determination of the fraction of free and hydrogen bonded carbonyl group can be calculated by the following equation:

$$f_b = \frac{A_b/a}{A_b/a + A_f}$$

A_f and A_b denote the areas corresponding to the free and hydrogen bonded carbonyl group, respectively. The conversion factor "*a*" is the specific absorption ratio of the above two bands. The value of $a = 1.5$ for the PVPh/PCL system was determined previously.[42] The results from curve fitting at room temperature are summarized in Table 2. These results indicate that the fraction of hydrogen bonded carbonyl groups is very less at low PVPh concentrations and also the value increases with increase in the PVPh content. From the FTIR data given in Figure 4 and Table 2, it can be seen that, up to 40 wt % of PVPh, the peak intensity and fraction of the hydrogen-bonded carbonyl groups are relatively less compared to the free carbonyl peak. The carbonyl groups of PCL block are less involved in hydrogen bonding in the

Table 2. Curve Fitting Results of PVPh Hydroxyl and PCL Carbonyl Interactions in PEO-*b*-PCL/PVPh Blends at 75 °C

	amorphous C=O			bonded C=O			
PEO-*b*-PCL/PVPh	v (cm^{-1})	$W_{1/2}$ (cm^{-1})	A_a (%)	v (cm^{-1})	$W_{1/2}$ (cm^{-1})	A_b (%)	f_b (%)
80/20	1735.5	15.57	28.82	1704.5	26.98	71.18	62.21
60/40	1735.1	17.81	58.2	1710.9	29.27	41.8	32.37
50/50	1735.3	16.39	64.9	1709.9	29.25	35.1	26.5
40/60	1735.6	17.26	81.26	1710.1	26.63	18.74	13.32
20/80	1735.8	18.89	94.75	1711.2	27.36	5.25	3.52
10/90	1735.4	17.82	98.28	1712.8	28.36	1.72	1.14

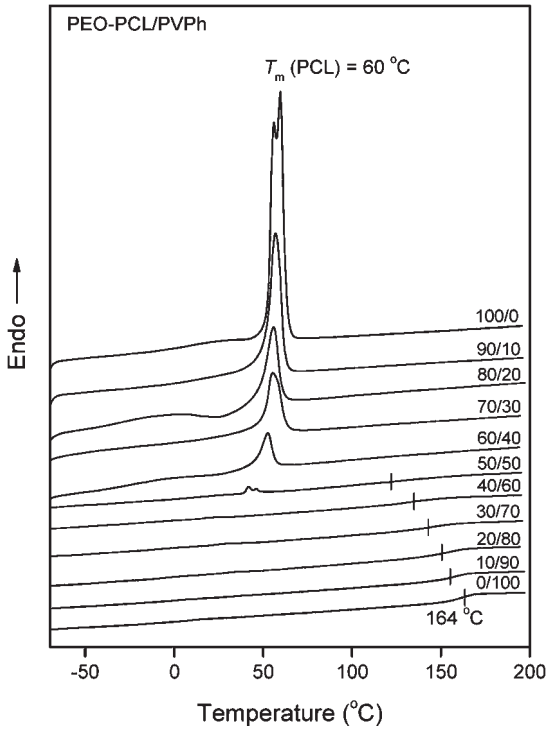

Figure 6. DSC thermograms of the second scan of PEO-*b*-PCL/PVPh blends.

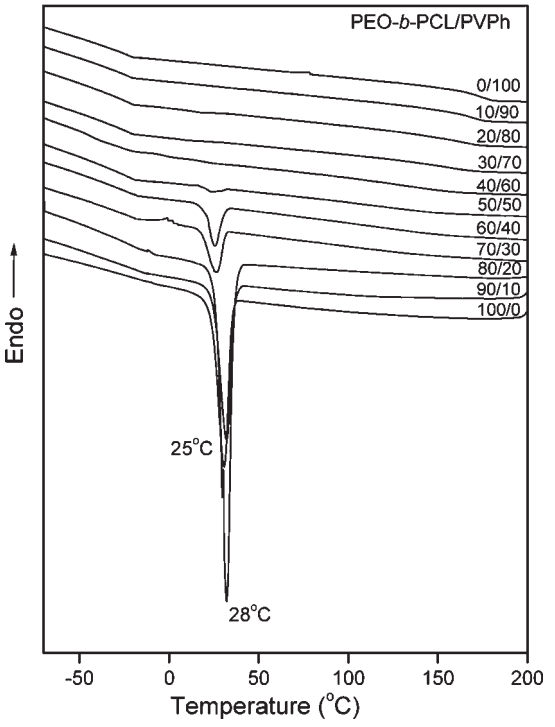

Figure 7. Crystallization curves of PEO-*b*-PCL/PVPh blends during cooling.

present block copolymer blend system compared with the PVPh/PCL homopolymer binary blends investigated by other authors.[43]

In the present PEO-*b*-PCL/PVPh blends, PCL block also forms hydrogen bonds with PVPh, and the average strength of these bonds increases with increasing PVPh concentration. The PCL block exhibits extensive hydrogen bonding with PVPh only when PVPh content reaches 40 wt % or above. This is due to the competitive hydrogen bonding interaction between PVPh/PEO blocks and PVPh/PCL blocks. Since the ability of PEO to form hydrogen bonds with PVPh is relatively high compared with PCL, the PEO blocks preferentially form high degree of hydrogen bonding with PVPh first.

It can be concluded from the FTIR results that strong hydrogen bonding between PEO and PVPh was observed in all the compositions. However, the carbonyl groups of PCL form less hydrogen bonding with PVPh hydroxyl groups at very low PVPh concentrations, and PCL interacts more strongly with PVPh at higher PVPh blends. In PEO-*b*-PCL/PVPh blends, competitive hydrogen bonding exists between the PVPh/PEO pair and PVPh/PCL pair at all compositions. Since the PVPh/PEO pair is relatively much stronger, PVPh/PCL hydrogen bonded pair exists weakly at lower PVPh concentration.

Phase Behavior and Crystallization. DSC experiments were performed to investigate the thermal properties of PEO-*b*-PCL/PVPh blends. Figures 6 and 7 show the DSC traces of PVPh, PEO-*b*-PCL, and their blends with various constituent compositions recorded by the heating and cooling scan, respectively. It is noted that a single T_g is the most widely and conventionally used criterion for the miscible blend. The pure block copolymer PEO-*b*-PCL should exhibit two T_gs corresponding to two immiscible blocks such as PEO and PCL. However, the T_gs of pure block copolymer components were not detectable under the present experimental conditions. It is noticeable that during heating and cooling run of DSC the crystallization and melting peaks were overlapped for samples with PEO-*b*-PCL due to the quite near T_c and T_m of both blocks. The binary blends of phenolic/PEO[39] and phenolic/PCL[44] are totally miscible over the entire compositions in the amorphous state due to interassociation hydrogen bonding between the hydroxyl group of phenolic and the carbonyl group of PCL and the ether group of PEO, respectively, though the T_gs of the blends PEO-*b*-PCL/PVPh show variations. The pure PVPh exhibits a T_g at 164 °C, which becomes broad and shifted down to lower temperatures in the blends as the block copolymer concentration was increased. This can be attributed to the miscibility between PVPh/PEO and PVPh/PCL components due to the formation of strong intermolecular hydrogen bonding interactions. Meanwhile, the melting temperatures of the block copolymer components in the blend decreases with an increasing content of the hydrogen bonding donor blocks.

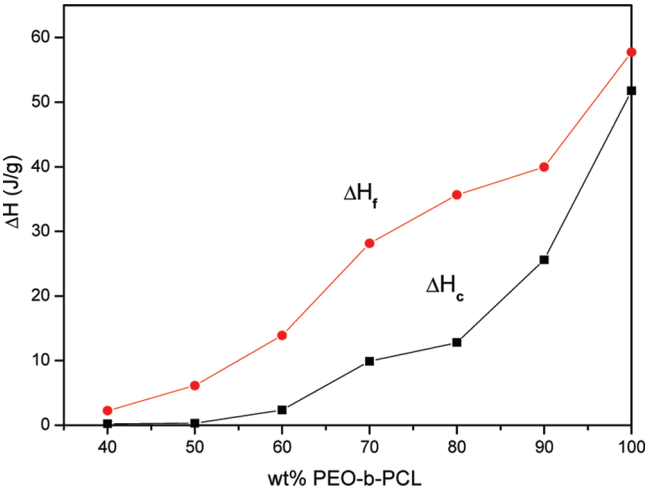

Figure 8. Heats of fusion (ΔH_f) and crystallization (ΔH_c) for PEO-*b*-PCL/PVPh blends.

Melting point depression is the characteristic of a miscible polymer blend involving hydrogen bonding interactions. The melting point depression of the crystalline components in the blends provides significant information about its miscibility and interaction behaviors. The pure PEO-*b*-PCL diblock copolymer exhibits two melting points, $T_{m\,(PEO)}$ = 60 °C and $T_{m(PCL)}$ = 56 °C, attributable to the crystalline PEO block and the crystalline PCL block, respectively. Figure 6 summarizes all the thermal transition temperatures from the heating scan as a function of the blend composition. The T_m of PEO disappears (or overlaps with the T_m of PCL), whereas that of PCL substantially shifts down to lower temperature with an increasing content of PVPh. It is clearly displayed that the T_m of PCL remains almost unchanged in the blends with very low PVPh concentration. This indicates that there is no high miscibility between PCL and PVPh at lower PVPh concentrations. The melting peak corresponding to the crystalline phases reduces in its intensity and eventually disappears at 50−60 wt % PVPh blends, and no melting peaks are observed thereafter, which is due to the miscibility of PCL and PEO with PVPh at higher PVPh contents.

The values of heats of fusion (ΔH_f) and crystallization (ΔH_c) for PEO-*b*-PCL/PVPh blends are plotted as a function of blend composition in Figure 8. These graphs indicate that at higher block copolymer concentration the heat of crystallization and melting temperature are very high, whereas the values go to zero when the PVPh content in the blends increases. This is because the overall crystallinity decreases due to the miscibility of PVPh with the block copolymer components. This may be attributed to the hydrogen bonding interaction of PEO and PCL components with PVPh. ΔH_f decrease is the indication of decreased crystallinity in the blends. But PEO-*b*-PCL/PVPh blends show a superposed melting (T_m) and crystallization (T_c) peak in the second heating as well as cooling; that is, both PCL and PEO blocks had similar maximal melting and crystallizing temperature.[45] Therefore, it is difficult to calculate the individual degrees of crystallinity of PCL and PEO. However, overall crystallinity of the block copolymer keeps decreasing as the concentration of PVPh increases in the blend.

DSC thermograms of cooling scan of PEO-*b*- PCL/PVPh blends are shown in Figure 7. The pure PEO-*b*-PCL block copolymer exhibits crystallization peak at 25 and 28 °C, whereas the blends show a crystallization peak higher than that of the block copolymer. The increase in crystallization

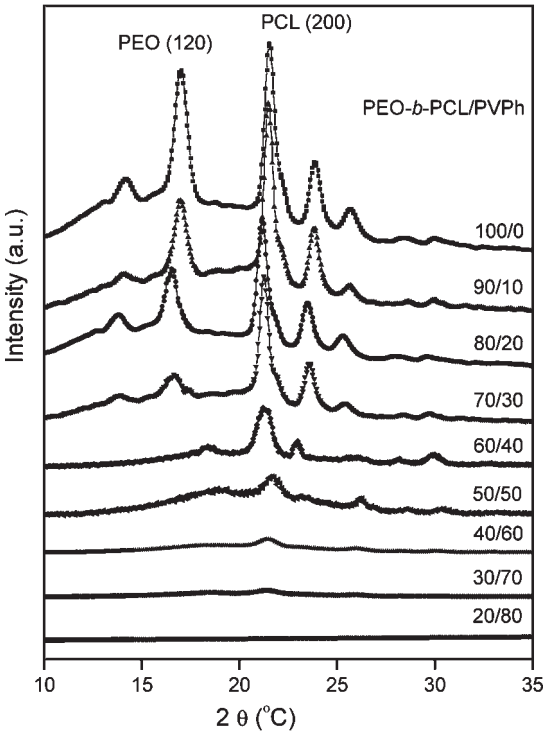

Figure 9. WAXD patterns of PEO-*b*-PCL/PVPh blends.

peak temperature upon the addition of PVPh may be due to the relaxation of PCL blocks of the block copolymer caused by the formation of strong hydrogen bonds between PEO and PVPh in lower PVPh content. This is due to the more favored formation of hydrogen bonds between PVPh and PEO rather than PVPh and PCL. These results are entirely consistent with the FTIR results described above.

The cast films of PEO-*b*-PCL/PVPh blends were also investigated using WAXS to study the effect of strong intermolecular interactions on the crystallographic orientation of PEO and PCL. Figure 9 shows the WAXS patterns of PEO-*b*-PCL/PVPh blends for different compositions at room temperature. The crystal systems of PEO and PCL are different since PEO has a monoclinic structure and PCL is orthorhombic. From the patterns in Figure 9, it can be seen that there are different diffraction peaks for both the PEO and PCL blocks, which correspond to the (120) plane peak of PEO crystallite and the (200) plane peak of PCL crystallite in the copolymer, indicating that both blocks are able to crystallize and form separate crystalline phases.

It is observed that the crystallization peak of PEO is lowered with increasing PVPh content, indicating the deterioration of the PEO crystalline structure. The introduction of PVPh content may cause the difference in the crystallographic orientation for the formation of the strong intermolecular interactions between PEO and PVPh. The WAXS patterns for the PEO-*b*-PCL/PVPh blends with 40 wt % PVPh show that the relative intensity of the (032) crystal plane is also smaller than that of the (120) crystal plane. The change in the crystallographic orientation of PEO in blends with another component forming strong intermolecular interactions may be the main factor for the slower growth rate of PEO. The crystalline order of PEO declines designates that the hydrogen bonding interactions of PEO with PVPh prevents its crystallization, which is in agreement with DSC results in Figures 6 and 7. Moreover, in PEO-*b*-PCL diblock copolymers, the crystallization ability of PEO block is restricted by the PCL block, which is covalently coupled to

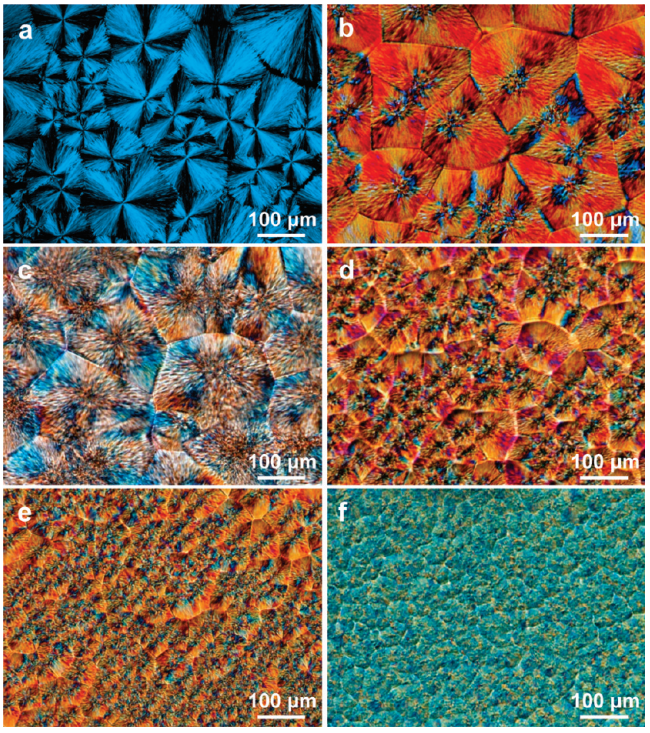

Figure 10. POM images of different PEO-*b*-PCL/PVPh blends at room temperature: (a) 100/0, (b) 90/10, (c) 80/20, (d) 70/30, (e) 60/40, and (f) 50/50 PEO-*b*-PCL/PVPh.

the other end of the PEO block. This indicates that there are two separated crystalline microdomains consisting of the PEO and PCL blocks in these diblock copolymers. This crystalline order of PCL also decreases once the PCL block starts to make hydrogen bonds with PVPh. Further increasing the PVPh content to 60−70 wt %, the crystallization peak of PCL disappears and results in amorphous halos in the WAXS because a large number of hydroxyl groups of PVPh form hydrogen bonding with carbonyl groups of PCL which inhibits the crystallization. In other words, the blend becomes miscible, and the crystalline structures of the PEO and PCL are destroyed. Further increasing the PVPh content, abundant PVPh becomes available to interact with both PEO and PCL through hydrogen bonding. By blending 70 wt % PVPh, the blends become miscible, and PVPh acts like a common solvent in this blend system. The WAXS results also show decreased crystallinity in the blends for both PCL and PEO blocks in accordance with the DSC results.

Blending of crystalline polymers with amorphous polymers induces changes in the crystallization such as depression in equilibrium melting temperature, decrease of crystallinity, and changes in semicrystalline morphology.[46] The polarizing optical micrographs of pure block copolymer and the blends are given in Figure 10. The THF cast films were analyzed at different magnifications. Spherulite attains different crystalline morphologies at different PEO-*b*-PCL compositions. In PEO-*b*-PCL/PVPh blends, as the concentration of PVPh increases, the size of spherulite becomes small. The POM picture of the pure PEO-*b*-PCL block copolymer is shown in Figure 10a. The spherulites of pure PEO display a "Maltese cross" birefringence pattern and have regular shape with defined borders. Comparing with the pure PEO and PCL, spherulites of the blends show a less regular texture. This is presumably because the noncrystallized materials such as PVPh and amorphous PEO and PCL are engulfed in interlamellar region as the crystallization of PEO and PCL proceeds, hence disturbing of the radial orientation and coarsening of the crystalline lamellae.[33] Figure 10b shows the spherulite morphology of 10 wt % PVPh blends, where the spherulite becomes less compact and differs significantly from that of neat PEO-*b*-PCL block copolymer. Apparently, PVPh effectively depresses the crystallizing tendency of PEO owing to stronger hydrogen bonding interactions or miscibility, whereas PCL has no strong interactions at lower PVPh concentrations. As the content of PVPh reaches 60 wt % (not given), there is no clear indication of crystalline structure; this indicates that the PCL blocks are miscible with PVPh, which restricts PCL from crystallization in these compositions. The morphologies obtained from POM seem to be a result of changes in the hydrogen bonding interactions between PVPh/PEO and PVPh/PCL. Hence, spherulite growth rate decreases with an increase in the content of the hydrogen bond donating polymer at a given value of crystallization temperature (T_c). Moreover, the degree of crystallinity was found to be lowered in blends in which both chains crystallized, which was speculated to be due to crystallization of one component reducing crystallization of the other within the same molecule.[33] Furthermore, the presence of hydrogen bond donating polymers in the blends with high values of T_g significantly decreases the rate of PEO and PCL crystallization, thereby reducing the spherulite growth. In general, there are three main factors dictating the depression of crystallization rate in the miscible crystalline polymers with high T_g: (1) a decrease of segmental mobility of the crystalline polymer transporting across the liquid−solid interface because of the high T_g of the homopolymer, (2) a dilution effect that reduces the number of crystallizable components at the surface of the growth spherulite, and (3) a decrease in supercooling resulting from the depression in melting point. It is established that the degree of supercooling is inversely proportional to the hydrogen bonding strength at a constant crystallization temperature. Therefore, the crystallization rate depression in the PEO-*b*-PCL/PVPh blends is consistent with the hydrogen bonding interaction strength.

Morphology. Block copolymers can self-assemble into a variety of ordered nanostructures due to microphase separation. This is driven by the enthalpy of demixing of the constituents of the block copolymer.[47] Since the block copolymers have covalent bond between them, they have a general tendency to separate, which results in microphase-separated structures. When a homopolymer is added to a diblock copolymer involving competitive hydrogen bonding, the less hydrogen bonded block is excluded from the homogeneous region due to the entropic penalty for conformational distortion. As to the polymer blends with both crystalline blocks, the morphology could be much complex than other binary blends system.

Figure 11a displays the structure of double crystalline PEO-*b*-PCL block copolymer observed by transmission electron microscopy (TEM). The plain block copolymer shows an ordered cubic structure in which spherical PEO nanophases are arranged in cubic lattices. The morphology of the PEO-*b*-PCL changes after the addition of homopolymer. Blends containing 20 wt % PVPh exhibit hexagonal cylindrical morphology with size in the order of ~40 nm (Figure 11b). Thus, it is obvious that the addition of PVPh can induce morphological transition in PEO-*b*-PCL self-assemblies. The shape of the micelles in blends was observed to change from hexagonal cylindrical to disordered bicontinuous phase as the PVPh concentration reaches 40 wt % (Figure 11c), which is a result of segregation of PCL blocks. Further increasing the PVPh content to 60 wt %, the polymer

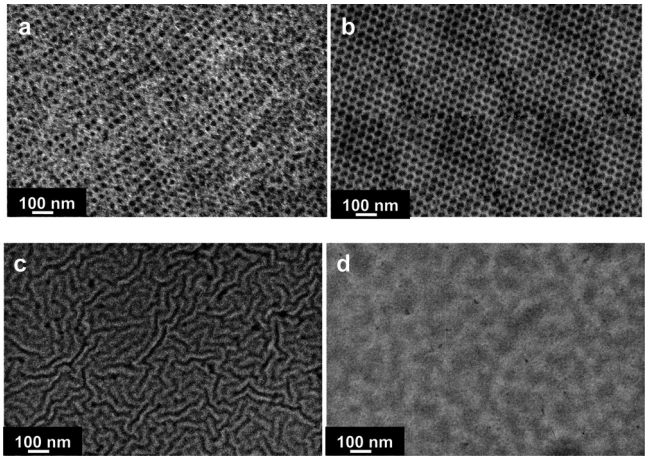

Figure 11. TEM micrographs of PEO-*b*-PCL/PVPh blends: (a) 100/0, (b) 80/20, (c) 60/40, and (d) 40/60 PEO-*b*-PCL/PVPh.

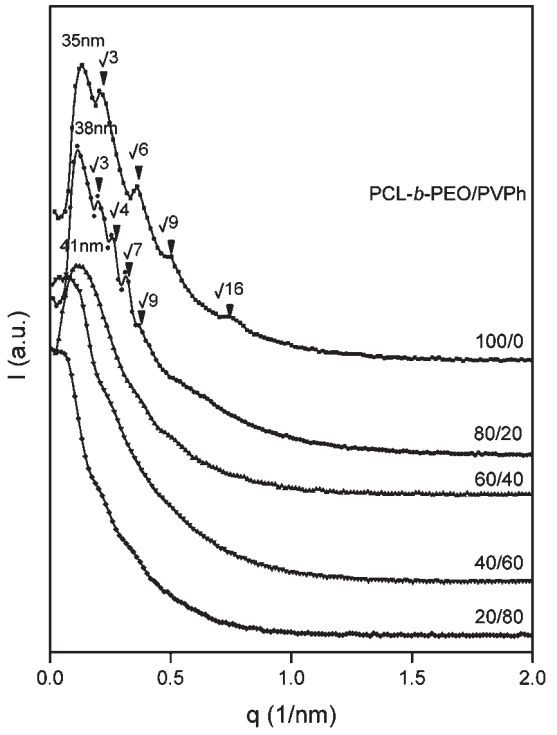

Figure 12. SAXS profiles of PEO-*b*-PCL/PVPh blends.

blend adopts a miscible or near-homogeneous morphology with no evidence of phase separation, illustrated in Figure 11d. As the content of PVPh is increasing further, the blends show completely homogeneous phase.

The ordered and disordered nanostructures in the PEO-*b*-PCL/PVPh blends were further investigated by small-angle X-ray scattering (SAXS). The SAXS profiles of the blends at room temperature are given in Figure 12. The microphase-separated morphology of the blends is clearly seen in the SAXS profiles. It is evident that the PEO-*b*-PCL block copolymer exhibits a scattering profile characteristic of ordered cubic structure with a long period of 35 nm corresponding to the spacing between neighboring PEO and PCL microdomains. The scattering peaks of the block copolymer situated at q values of $1:\sqrt{3}:\sqrt{6}:\sqrt{9}:\sqrt{16}$ relative to q^* are apparent. This can be attributed to the lattice scattering peaks of spherical (or cylindrical) nanophases arranged in cubic lattices such as body-centered cubic (bcc), face-centered cubic (fcc),

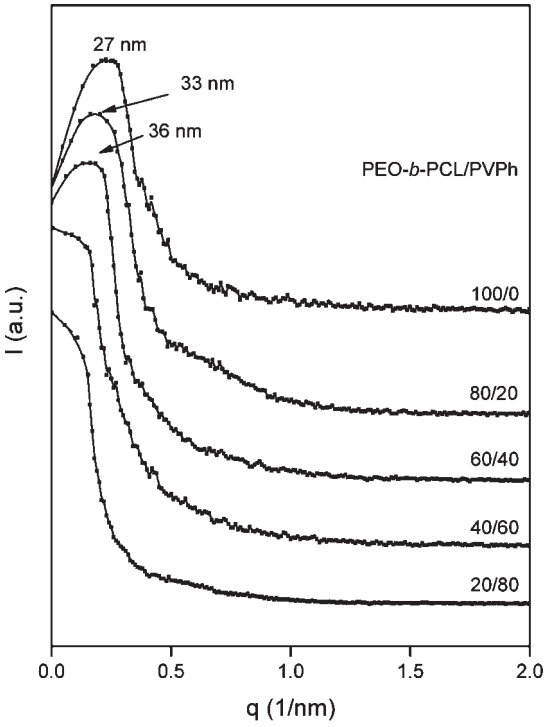

Figure 13. SAXS profiles of PEO-*b*-PCL/PVPh blends at 100 °C.

or simple cubic symmetries. Moreover, the cubic morphology of the PEO-*b*-PCL block copolymer was already revealed in TEM observations. The 20 wt % PVPh blend shows a well-ordered hexagonally packed cylindrical profile ($q/q^* = 1:\sqrt{3}:\sqrt{4}:\sqrt{7}:\sqrt{12}$), which is also in consistent with the TEM images. The blends with 40 wt % PVPh give broad peaks, and the broadening of the peak indicates the deterioration of long-range ordered structures. The average spacing between the neighboring microdomains is 38 and 41 nm for 20 and 40 wt % PVPh blends, respectively. This result shows that there is a systematic increase in the size of the phase-separated domain which implies the progressive incorporation of PVPh. Above 40 wt % PVPh, the blends show only weak and broad peaks, indicating a near-homogeneous morphology as observed in 60 and 80 wt % PVPh blends in Figure 12.

The SAXS measurements were also performed at 100 °C above the melting point of the block copolymer components, and the results are shown in Figure 13. At 100 °C, where both PCL and PEO blocks are amorphous, broad scattering peaks are observed, indicating that there are no ordered structures; i.e., neither crystalline lamellae nor ordered microphases existed in the melts. At higher temperature, the crystalline PCL and PEO lamellae became the melt, and therefore PVPh can be located in both the PEO and PCL domains. Moreover, an ordered-to-disordered transition of the microphase morphology took place upon heating, and the order−disorder transition temperature is lower than 100 °C. This is revealed by disappearance of the ordered cubic phase for the pure block copolymer and the hexagonal cylindrical morphology for the blend with 20 wt % PVPh. The blends all display disordered microphase morphology at 100 °C. It can be seen from Figure 13 that the primary scattering peak of all the samples shifts to larger q value positions and broadens to some extent, and thus the average distance between neighboring microdomains decreases.

The mechanism of formation of different microphases and nanostructures in PEO-*b*-PCL/PVPh blends at different compositions is schematically summarized in Figure 14.

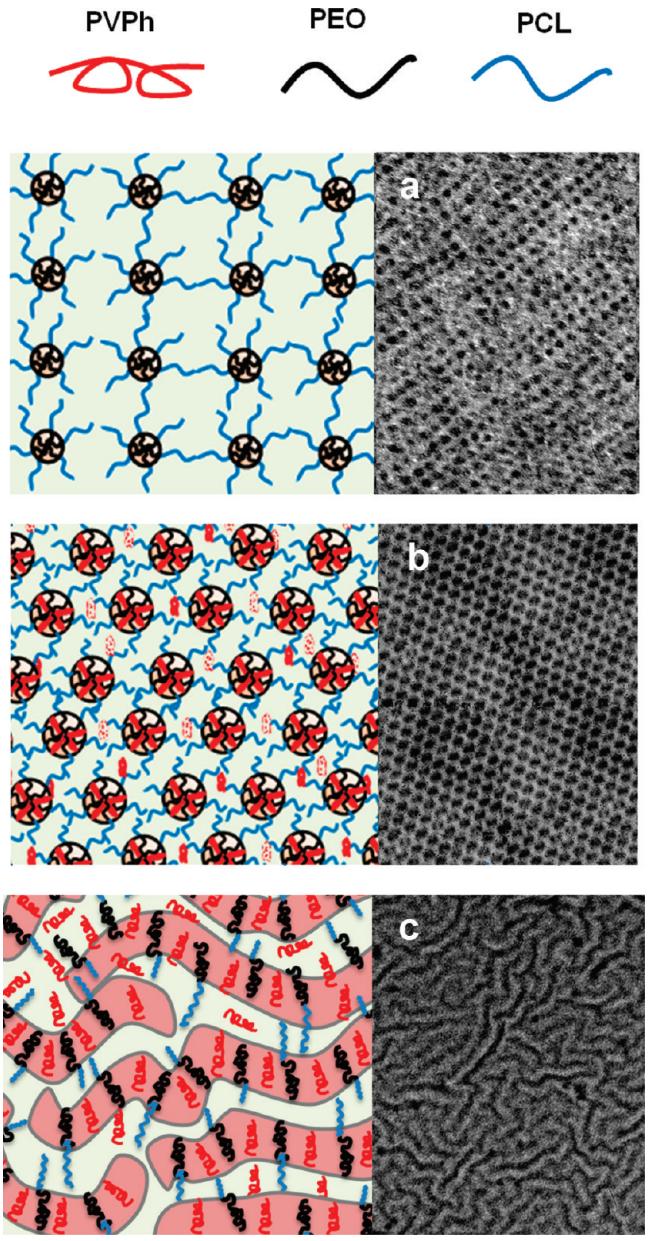

Figure 14. Schematic representation of phase morphologies in PEO-*b*-PCL/PVPh blends: (a) cubical micelles of PEO-*b*-PCL block copolymer, (b) hexagonal cylindrical micelles at 20 wt % PVPh concentration, and (c) disordered lamellae at 40 wt % PVPh concentration.

The blends include an immiscible block copolymer PEO-*b*-PCL and a homopolymer PVPh, which is miscible with both PEO and PCL blocks depending on the concentration. The pure diblock copolymer exhibits a cubic structure. The block copolymers have the general tendency to separate. They exhibit amphiphilic characteristic which is caused by the restriction due to the presence of a covalent bond between the chemically different blocks, resulting in microphase-separated structures. The 20 wt % PVPh blends show a cylindrical morphology. At 20 wt %, the added PVPh and PEO interacts very strongly, whereas PCL blocks, which are repelled by PEO, have weak association with PVPh. The added PVPh which strongly hydrogen bonded with PEO form PVPh/PEO single phase cylinders inside whereas the weakly interacting PVPh/PCL phase, as shown in Figure 14b. At very low concentration, PVPh forms a strong hydrogen bond with PEO and as such acts as a selective amphiphilic solvent for the PEO blocks of the PEO-*b*-PCL block copolymer. For the pure block copolymer, which is originally in the cubical phase, the addition of PVPh is thus expected to induce structural transformations, in analogy with block copolymer selective solvent systems.[32] In 40 wt % PVPh blends, the concentration of homopolymer, as well as PVPh/PEO single phase, increases, whereas PCL also forms hydrogen bonds with PVPh. This competitive hydrogen bonding destructs the ordered structure of the block copolymer. This leads to the decrease in the interfacial area, which results in the planar interfaces and thereby the formation of disordered bicontinuous phase, as shown in Figure 14c. At 60 wt % or above PVPh blends, more PCL forms hydrogen bonds with PVPh, or in other words, both PEO and PCL blocks are miscible with PVPh to form homogeneous morphology. Since the concentration of PVPh is very high compared to that of block copolymer, though there exists a strong interaction between PEO and PVPh, the increased amount of PVPh results in hydrogen bonding interactions with PCL as well due to the availability of free hydroxyl groups resulting in homogeneous morphology. The different nanostructures observed in these blends are completely different from the cubical microphase of the pure PEO-*b*-PCL block copolymer, implying that the PEO blocks are actually swollen when PVPh is added. In the present case, hydrogen bonds clearly form the dominant interaction in the blend where PVPh/PEO hydrogen bonds are found to be stronger than PVPh/PVPh and PVPh/PCL hydrogen bonds.

In the current work, we investigated the selective hydrogen bonding in PEO-*b*-PCL/PVPh blends, wherein both the blocks are miscible with the PVPh depending on the concentration of the latter. Here, the value of χ_{AB} is positive (A and B are immiscible), and χ_{AC} and χ_{BC} are negative, but χ_{AC} is more negative than χ_{BC}. Here, the connectivity of the immiscible blocks prevents macrophase separation, and instead, a structure forms with microphase sized A- and B-rich regions separated by an extensive amount of internal interface. The length scale of this microstructure is determined by a competition between the interface tension, which favors large domain sizes, and the entropic stretching energy of the polymers, which prefers small domains. The addition of a homopolymer to the block copolymer provides new behavior. This will effect different phases to varying degrees; it can alter their relative stabilities and bring about new equilibrium structures. The morphological variations of this system is shown to be influenced by two factors: (1) intermolecular interaction between PVPh and PEO is stronger than that between PVPh and PCL, which indicates the existence of competitive hydrogen bonding, and (2) formation of a homogeneous phase of PVPh/PEO which excludes microdomains of weakly interacted PCL. So the geometry of the structures formed in the blends is determined to a large extent by the competition between the PEO and PCL blocks in regards to hydrogen bonding with PVPh. Moreover, it is also established that the addition of a homopolymer into to an ordered block copolymer will cause changes in the microdomain structure.

Conclusions

We have observed the microphase separation mediated by competitive hydrogen bonding in PEO-*b*-PCL/PVPh double crystalline diblock copolymer/homopolymer blends. The hydroxyl groups of PVPh can selectively interact with both ether groups of PEO and carbonyl groups of PCL, which leads to the formation of composition-dependent microphase-separated morphologies in these blends. The disparity of weakly associated

PVPh/PCL pairs and strongly associated PVPh/PEO pairs results in microphase separation and the formation of cubic, hexagonal cylindrical morphologies at lower PVPh concentrations. The PVPh can act as a common solvent for both of the blocks at higher concentrations which results in disordered and homogeneous blends at high PVPh contents. The formation of various composition-dependent microphase-separated morphologies in the PEO-*b*-PCL/PVPh blends can be explained based on the relative strength of hydrogen bonding between the different pairs in the system.

Acknowledgment. The authors thank AINSE Ltd. for providing financial assistance to enable work on SAXS to be conducted.

References and Notes

(1) Terreau, O.; Bartels, C.; Eisenberg, A. *Langmuir* **2004**, *20* (3), 637.
(2) Jain, S.; Bates, F. S. *Macromolecules* **2004**, *37*, 1511.
(3) Park, M.; Harrison, C.; Chaikin, P. M.; Register, R. A.; Adamson, D. H. *Science* **1997**, *276*, 1401.
(4) Muthukumar, M.; Ober, C. K.; Thomas, E. L. *Science* **1997**, *27*, 1225.
(5) (a) Hamley, I. U. *The Physics of Block Copolymers*; Oxford University Press: Oxford, UK, 1998.(b) Foerster, S.; Antonietti, M. *Adv. Mater.* **1998**, *10*, 195. (c) Hadjichristidis, N.; Pispas, S.; Floudas, G. A. *Block Copolymers Synthetic Strategies, Physical Properties, and Applications*; John Wiley & Sons: Hoboken, NJ, 2003.
(6) Kataoka, K.; Harada, A.; Nagasaki, Y. *Adv. Drug Delivery Rev.* **2001**, *47*, 113.
(7) Rosler, A.; Vandermeulen, G. W. M.; Klok, H. A. *Adv. Drug Delivery Rev.* **2001**, *53*, 95.
(8) Riess, G.; Hurtrez, G.; Bahadur, P. *Block Copolymers*, 2nd ed.; Wiley: New York, 1985, p 324.
(9) Nace, V. M. *Nonionic Surfactants: Polyoxyalkylene Block Copolymers*; Surfactant Science Series 60; Marcel Dekker: New York, 1996; p 1.
(10) Alexandris, P.; Lindman, B. *Amphiphilic Block Copolymers: Self-Assembly and Applications*; Elsevier: Amsterdam, 2000; Vol. *1*, p 435.
(11) Price, C. Colloidal Properties of Block Copolymers. In *Developments in Block Copolymers 1*; Goodman, I., Ed.; Applied Science: London, 1982; p 39.
(12) Piirma, I. *Polymeric Surfactants*; Surfactant Science Series 42; Marcel Dekker: New York, 1992; p 1.
(13) Tuzar, Z.; Kratochvil, P. Micelles of Block and Graft Copolymers in Solution. In *Surface and Colloid Science*; Matijevic, E., Ed.; Plenum Press: New York, 1993; Vol. *15*, Chapter 1, pp 1−83.
(14) Riess, G.; Hurtrez, G.; Bahadur, P. Block Copolymers. In *Encyclopedia of Polymer Science and Engineering*, 2nd ed.; Wiley: New York, 1985; Vol. *2*, pp 324−434.
(15) Webber, S. E.; Munk, P.; Tuzar, Z. *Solvents and Self-Organization of Polymer*; NATO ASI Series, Series E: Applied Sciences; Kluwer Academic Publisher: Dordrecht, 1996; Vol. *327*, p 1.
(16) Alexandridis, P.; Hatton, T. A. Block Copolymers. In *Polymer Materials Encyclopedia 1*; CRC Press: Boca Raton, FL, 1996; p 743.
(17) Nace, V. M. *Nonionic Surfactants: Polyoxyalkylene Block Copolymers*; Surfactant Science Series 60; Marcel Dekker: New York, 1996; p 1.
(18) Hamley, I. W. In *The Physics of Block Copolymers*; Hamley, I. W., Ed.; Oxford Science Publication: New York, 1998; p 131.
(19) Alexandridis, P.; Lindman, B. *Amphiphilic Block Copolymers: Self-Assembly and Applications*; Elsevier: Amsterdam, 2000; p 1.
(20) Riess, G.; Dumas, P. H.; Hurtrez, G. *Block Copolymer Micelles and Assemblies*; MML Series 5; Citus Books: London, 2002; pp 69−110.
(21) Xie, H. Q.; Xie, D. *Prog. Polym. Sci.* **1999**, *24*, 275.
(22) Gohy, J. F.; Varshney, S. K.; Jerome, R. *Macromolecules* **2001**, *34*, 3361.
(23) Nakashima, K.; Bahadur, P. *Adv. Colloid Interface Sci.* **2006**, *123*, 75.
(24) Ruokolainen, J.; Saariaho, M.; Ikkala, O.; ten Brinke, G.; Thomas, E. L.; Torkkeli, M. *Macromolecules* **1999**, *32*, 1152.
(25) (a) Hameed, N.; Guo, Q. *Polymer* **2008**, *49*, 5268. (b) Guo, Q. *Thermochim. Acta* **2006**, *451*, 168.
(26) Abetz, V.; Goldacker, T. *Macromol. Rapid Commun.* **2000**, *21*, 16.
(27) (a) Hu, Z.; Jonas, A. M.; Varshney, S. K.; Gohy, J. F. *J. Am. Chem. Soc.* **2005**, *127*, 6526. (b) Lefevre, N.; Fustin, C. A.; Gohy, J. F. *Langmuir* **2007**, *23*, 4618. (c) Hu, Z.; Verheijen, W.; Hofkens, J.; Jonas, A. M.; Gohy, J. F. *Langmuir* **2007**, *23*, 116.
(28) (a) Kuo, S. W.; Chang, F. C. *Macromolecules* **2001**, *34*, 4089. (b) Lee, H. F.; Kuo, S. W.; Huang, C. F.; Lu, J. S.; Chan, S. C.; Wang, C. F.; Chang, F. C. *Macromolecules* **2006**, *39*, 5458.
(29) (a) Kosonen, H.; Ruokolainen, J.; Nyholm, P.; Ikkala, O. *Macromolecules* **2001**, *34*, 3046. (b) Ruokolainen, J.; Mäkinen, R.; Torkkeli, M.; Mäkelä, T.; Serimaa, R.; ten Brinke, G.; Ikkala, O. *Science* **1998**, *280*, 557. (c) van Zoelen, W.; van Ekenstein, G. A.; Ikkala, O.; ten Brinke, G. *Macromolecules* **2006**, *39*, 6574. (d) Mäki-Ontto, R.; de Moel, K.; Polushkin, E.; van Ekenstein, G. A.; ten Brinke, G.; Ikkala, O. *Adv. Mater.* **2002**, *14*, 357.
(30) (a) Hameed, N.; Guo, Q. *Polymer* **2008**, *49*, 922. (b) Hameed, N.; Liu, J.; Guo, Q. *Macromolecules* **2008**, *1*, 7596. (c) Salim, N. V.; Hameed, N.; Guo, Q. *J. Polym. Sci., Part B: Polym. Phys.* **2009**, *47*, 1894.
(31) (a) Chen, W. C.; Kuo, S. W.; Lu, C. H.; Jeng, U. S.; Chang, F. C. *Macromolecules* **2009**, *42*, 3580. (b) Chen, W. C.; Kuo, S. W.; Jeng, U. S.; Chang, F. C. *Macromolecules* **2008**, *41*, 1401. (c) Chen, S. C.; Kuo, S. W.; Jeng, U. S.; Su, C. J.; Chang, F. C. *Macromolecules* **2010**, *43*, 1083.
(32) Hamley, I. W. *The Physics of Block Copolymers*; Oxford University Press: Oxford, UK, 1998.
(33) Loewenhaupt, B.; Steurer, A.; Hellmann, G. P.; Gallot, Y. *Macromolecules* **1994**, *27*, 908.
(34) Matsen, M. W. *Macromolecules* **1995**, *28*, 5765.
(35) Hameed, N.; Salim, N. V.; Guo, Q. *J. Chem. Phys.* **2009**, *131*, 214905.
(36) (a) Etxeberria, A.; Guezala, S.; Iruin, J. J.; Campa, J. G.; Abajo, J. D. *Polymer* **1998**, *39*, 1035. (b) Mekhilef, N.; Hadjiandreou, P. *Polymer* **1995**, *36*, 2165. (c) Qin, C.; Pires, A. T. N.; Belfiore, L. A. *Macromolecules* **1991**, *24*, 666. (d) Coleman, M. M.; Yang, X.; Painter, P. C.; Graf, J. F. *Macromolecules* **1992**, *25*, 4414.
(37) (a) Purcell, K. F.; Drago, R. S. *J. Am. Chem. Soc.* **1968**, *89*, 2874. (b) Guo, Q.; Harratsa, C.; Groeninckx, G.; Koch, M. H. J. *Polymer* **2001**, *42*, 4127. (c) Guo, Q.; Harratsa, C.; Groeninckx, G.; Reynaers, H.; Koch, M. H. J. *Polymer* **2001**, *42*, 6031.
(38) Moskala, E. J.; Varnell, D. F.; Coleman, M. M. *Polymer* **1985**, *26*, 228.
(39) Kuo, S. W.; Chang, F. C. *Macromol. Chem. Phys.* **2001**, *202*, 3112.
(40) Chintapalli, S.; Frech, R. *Macromolecules* **1996**, *29*, 3499.
(41) (a) Coleman, M. M.; Graf, J. F.; Painter, P. C. *Specific Interactions and the Miscibility of Polymer Blends*; Technomic Publishing: Lancaster, PA, 1991. (b) Coleman, M. M.; Painter, P. C. *Prog. Polym. Sci.* **1995**, *20*, 1.
(42) (a) Kuo, S. W.; Huang, C. F.; Chang, F. C. *J. Polym. Sci., Part B: Polym. Phys.* **2001**, *39*, 1348. (b) Cesteros, L. C.; Meaurio, E.; Katime, I. *Macromolecules* **1993**, *26*, 2323.
(43) Coleman, M. M.; Graf, J. F.; Painter, P. C. *Specific Interactions and the Miscibility of Polymer Blends*; Technomic Publishing: Lancaster, PA, 1991.
(44) Crescenzi, V.; Manzini, G.; Calzolari, G.; Borri, C. *Eur. Polym. J.* **1972**, *8*, 449.
(45) He, C. L.; Sun, J. R.; Zhao, T.; Hong, Z. K.; Zhuang, X. L.; Chen, X. S.; Jing, X. B. *Biomacromolecules* **2006**, *7*, 252.
(46) Ong, C. J.; Price, F. P. *J. Polym. Symp.* **1978**, *63*, 45.
(47) Chen, H. L.; Wu, J. C.; Lin, T. L.; Lin, J. S. *Macromolecules* **2001**, *34*, 6936.